

Counter-Gradient Momentum Transport Through Subtropical Shallow Convection in ICON-LEM Simulations

Dixit, Vishal; Nuijens, Louise; Helfer, Kevin C.

DOI

[10.1029/2020MS002352](https://doi.org/10.1029/2020MS002352)

Publication date

2021

Document Version

Final published version

Published in

Journal of Advances in Modeling Earth Systems

Citation (APA)

Dixit, V., Nuijens, L., & Helfer, K. C. (2021). Counter-Gradient Momentum Transport Through Subtropical Shallow Convection in ICON-LEM Simulations. *Journal of Advances in Modeling Earth Systems*, 13(6), 1-20. Article e2020MS002352. <https://doi.org/10.1029/2020MS002352>

Important note

To cite this publication, please use the final published version (if applicable). Please check the document version above.

Copyright

Other than for strictly personal use, it is not permitted to download, forward or distribute the text or part of it, without the consent of the author(s) and/or copyright holder(s), unless the work is under an open content license such as Creative Commons.

Takedown policy



Please contact us and provide details if you believe this document breaches copyrights. We will remove access to the work immediately and investigate your claim.



RESEARCH ARTICLE

10.1029/2020MS002352

Counter-Gradient Momentum Transport Through Subtropical Shallow Convection in ICON-LEM Simulations

 Vishal Dixit¹ , Louise Nuijens¹, and Kevin C. Helfer¹ 
¹Department of Remote Sensing and Geosciences, TU Delft, Delft, the Netherlands**Key Points:**

- Shallow convective momentum transport decelerates northeasterly trade winds below cloud base and favors nonlocal, counter-gradient momentum flux near cloud-tops
- The counter-gradient momentum transport is arbitrated by horizontal circulations surrounding the clouds driven by cross-cloud pressure gradients
- Analysis of conditional sampling through clouds confirm their small contribution to counter-gradient fluxes and a so-called “cumulus friction”

Supporting Information:

Supporting Information may be found in the online version of this article.

Correspondence to:V. Dixit,
v2dixit@gmail.com**Citation:**

Dixit, V., Nuijens, L., & Helfer, K. C. (2021). Counter-gradient momentum transport through subtropical shallow convection in ICON-LEM simulations. *Journal of Advances in Modeling Earth Systems*, 13, e2020MS002352. <https://doi.org/10.1029/2020MS002352>

Received 25 SEP 2020
Accepted 4 MAY 2021

Abstract It is well known that subtropical shallow convection transports heat and water vapor upwards from the surface. It is less clear if it also transports horizontal momentum upwards to significantly affect the trade winds in which it is embedded. We utilize unique multiday large-eddy simulations run over the tropical Atlantic with ICON-LEM to investigate the character of shallow convective momentum transport (CMT). For a typical trade-wind profile during boreal winter, CMT acts as an apparent friction to decelerate the north-easterly flow. This effect maximizes below the cloud base while in the cloud layer, friction is very small, although present over a relatively deep layer. In the cloud layer, the zonal component of the momentum flux is counter-gradient and penetrates deeper than reported in traditional shallow cumulus LES cases. The transport through conditionally sampled convective updrafts and downdrafts explains a weak friction effect, but not the counter-gradient flux near the cloud tops. The analysis of the momentum flux budget reveals that, in the cloud layer, the counter-gradient flux is driven by convectively triggered nonhydrostatic pressure-gradients and horizontal circulations surrounding the clouds. A model set-up with large domain size and realistic boundary conditions is necessary to resolve these effects.

Plain Language Summary The vertical profile of temperature and moisture is strongly controlled by atmospheric moist convection as it mixes heat and water vapor upwards from the surface. It is less clear if it also mixes horizontal momentum upwards to significantly affect the vertical profile of winds. Past studies have found that the subtropical-shallow convection mainly transports momentum down-gradient so as to reduce the vertical wind shear. We utilize unique multiday large-eddy simulations run over the tropical Atlantic under the German HD(CP)² project to quantify the convective momentum transport. We find that for a typical trade wind profile, convection acts like a friction on the surrounding flow below cloud base while near cloud tops it transports momentum so as to enhance the vertical shear in the mean wind. Detailed analysis of momentum fluxes indicates that the convectively driven turbulent circulations around the clouds facilitate this transport. This mechanism of momentum transport is typically not included in most climate models and may have fundamental implications for simulations of the trade winds.

1. Introduction

It has been known since the 1960s that atmospheric convection transports water vapor and heat upwards in the troposphere from the surface (Riehl, 1958). This happens as convection, acting through mesoscale and sub-mesoscale updrafts and downdrafts, carries heat and moisture vertically. But it is still not clear to what extent convection transports horizontal momentum upwards to either accelerate or decelerate the tropospheric flows. Within the theme of cloud-circulation coupling, which has been identified as a key limiter in our understanding of future climate changes (Bony et al., 2015), convective momentum transport (CMT) is an unexplored mechanism. Here, we have investigated the processes that control the character of CMT through subtropical shallow convection.

Understanding CMT is challenging because unlike heat or scalar field transport, horizontal momentum is not necessarily conserved during mass transport. Instead, the momentum is continually exchanged with the environment through other mechanisms such as pressure perturbations that trigger horizontal circulations around updrafts and downdrafts and form drag.

© 2021. The Authors. Journal of Advances in Modeling Earth Systems published by Wiley Periodicals LLC on behalf of American Geophysical Union. This is an open access article under the terms of the [Creative Commons Attribution-NonCommercial License](https://creativecommons.org/licenses/by-nc/4.0/), which permits use, distribution and reproduction in any medium, provided the original work is properly cited and is not used for commercial purposes.

The measurements of pressure perturbations in and across convecting entities are difficult. Despite this difficulty, some isolated observations have been made (e.g., LeMone, 1983; LeMone & Moncrieff, 1994). LeMone (1983) observed CMT occurring through lines of cumulonimbus clouds. Her results suggested that the flux of convective momentum was of similar sign as that of mean large-scale wind shear indicating a counter-gradient transport. Traditionally, one thinks of “down-gradient” momentum transport as mixing away of shear, while “counter-gradient” (or “up-gradient”) momentum transport is thought to enhance wind shear. This implied that lines of cumulonimbus clouds favor nonlocal transport in the direction opposite to the shear-driven, down-gradient turbulent mixing. A more comprehensive study later also presented cases where down-gradient transport was stronger than the nonlocal CMT (LeMone et al., 1984). Similarly, Wu and Yanai (1994) found down-gradient transport in their analysis of residues in the momentum budget calculated from measurements obtained for deep convection during the TOGA COARE campaign. From these handful of observational studies, it is not clear if shallow CMT is down-gradient or counter-gradient.

The landmark study of Schneider and Lindzen (1976) provided an initial impetus for the study and parameterization of CMT in general circulation models. They were motivated by the fact that moist convection acts as a link between viscous flow in the turbulent boundary layer and relatively friction-free fast-moving free tropospheric air above it. This led them to propose that clouds and convection originating near the surface mainly act as a “cumulus friction” on the free tropospheric flow. Some researchers since then have proposed parameterizations to account for this effect in climate models (Gregory et al., 1997; Romps, 2012; Kershaw & Gregory, 1997; Wu & Yanai, 1994; Zhang & Cho, 1991). These studies mainly used conclusions from observations (LeMone & Moncrieff, 1994) or cloud-resolving models (CRMs; ~ 1 km resolution) to propose modifications to convective parameterizations that account for pressure perturbations. They did not derive if clouds in general act as a cumulus friction on the surrounding flows and have focused only on deep convection.

A significant body of literature has focused on parameterizing the observed “mesoscale organization” of multilayered convective systems (e.g., Moncrieff, 1981, 1992, 2019). The momentum transport through “organized convection” such as shear-perpendicular or shear-parallel systems (Grant et al., 2020), is thought to be fundamentally distinct from turbulent mixing, and has been shown to favor down-gradient or counter-gradient momentum transport in distinct atmospheric layers (Moncrieff, 1992). An archetypal model based on slantwise overturning circulations associated with these systems has been proposed, as these are typically not addressed by the traditional CMT parameterizations (Moncrieff, 2010; Moncrieff et al., 2017; Moncrieff & Liu, 2006). When implemented in either weather or climate models, they have been shown to improve the simulation of tropical convection. Recently, new geometries of purely shallow convective organization such as “Fish”, “Gravel”, “Flower”, and “Sugar” have been identified in the trade wind regions (Bony et al., 2020; Rasp et al., 2020; Stevens et al., 2020). It is an open question if these organized shallow convective systems transport momentum similar to their deep convective counterparts.

It may be intuitive to expect that more vigorous deep convection promotes stronger CMT. However, it is hard to overlook the fact that shallow convection is more frequent and all pervasive in the tropics. Interestingly, indirect attempts to diagnose CMT support this view as well. Carr and Bretherton (2001) used reanalysis data to compute the vertical profile of CMT as a residue in the large-scale budget of the horizontal momentum. They found large residues only in the lower troposphere, suggesting that shallow CMT may well have a larger role in the momentum budget of large-scale circulations than deep CMT.

There are a few recent studies that have used large-eddy simulations (LES, ~ 100 m resolution) with idealized boundary conditions to analyze CMT through shallow convection. The LES has an advantage over CRMs (~ 1 km resolution) because scales of shallow convective motions are better resolved in the former. Brown (1999), using LES simulations of BOMEX at ~ 100 m resolution, showed that the vertical momentum flux is a strong function of the background wind shear in their simulations. Zhu (2015) studied various shallow convection cases (e.g., BOMEX, RICO, DYCOMS, and ASTEX) and reported that a significant CMT occurs through the small-scale turbulent motions not resolved at 100 m resolution. However, contributions from large-scale eddies were equally significant in their simulations. Furthermore, the relative contributions from small/large eddies changed depending on the case in their study. Schlemmer et al. (2017) noted mainly down-gradient momentum fluxes in their simulations of RICO. In contrast, Larson et al. (2019) found counter-gradient momentum flux in a thin layer near cloud base in their simulations of BOMEX.

They showed that the counter-gradient flux is driven by the cross-correlations of buoyancy with the perturbation vertical velocity in their model. Badlan et al. (2017) used LES to simulate deep convection and showed that convection simulated with idealized doubly periodic boundary conditions may not simulate the natural growth of deep convective systems. Furthermore, they found that the properties of CMT were sensitive to the domain size. This suggests that a proper aspect ratio of the domain is needed to adequately simulate the convective circulations. Most of the LES studies focusing on shallow CMT utilized simulations with idealized boundary conditions or were integrated over a small domain (~ 25 km). It is not clear how such idealizations influence the conclusions they report.

This study aims to investigate the character of shallow CMT (downgradient or counter-gradient) using the state of the art, large-domain, long-time integrations of the ICON large-eddy model (ICON-LEM) over the tropical North Atlantic. These LES utilize a nested simulation strategy, derive boundary conditions from the outer model domain, and are run for longer time periods than past studies. We first describe the ICON-LEM simulation set-up and methods of analysis in Section 2. Then the results are presented in Section 3, and finally discussion and conclusions are presented in Sections 4 and 5, respectively.

2. Simulations and Analysis

2.1. ICON-LEM Simulations

Under the German HD(CP)² (High-Definition Clouds and Precipitation for Advancing Climate Predictions) project; simulations were run over the Atlantic ocean using the Icosahedral Nonhydrostatic model (ICON) (Dipankar et al., 2015; Zängl et al., 2015) to study subtropical shallow clouds. This set of simulations was run at multiple resolutions covering a wide area over the tropical Atlantic and served as a hind-cast for the NARVAL (Next-Generation Aircraft Remote Sensing for Validation) observational expedition (Klocke et al., 2017; Stevens et al., 2019). Within this cascade of simulations, the coarse model is run at cloud-resolving resolutions of about 1.25 km while the finest model is run at 150 m resolution in the innermost domain.

The simulations were run over 6 days from December 11 to 19, 2013 (11, 12, 14, 15, 16, December 20, 2013). Each simulation was run for 27 h starting at 9 UTC. The first 3 h were discarded as spin-up on all days in the presented analysis. The lateral boundary conditions were obtained from the outer LES run at coarser resolution and were nudged every hour using a one-way nesting. The boundary conditions for the outermost model were forced using ECMWF reanalysis data (Dee et al., 2011). A time-step of 1.5 s was used for the 150 m resolution run. The LES runs used a binary cloud scheme and Smagorinsky sub-grid scale turbulence scheme. The output for instantaneous fields every 15 min was made available on the Icosahedral grid which was converted to a lat-lon grid using regriding functions available with the CDO package (weights for the geographic grid were generated using “genycon” and then the output was remapped with “remap”) as recommended in the ICON manual (Prill et al., 2019).

We utilized the ICON-LEM with the finest horizontal grid resolution of 150 m which covers a 200×100 km² area out of which we sampled from a 100×100 km² area centered at 13.1°N and 58.5°E with 150 vertical levels. This area was selected to minimize the effect of lateral nudging at the longitudinal boundaries. To test the effect of domain size on the analysis, we repeated the analysis sampling from increasingly smaller domains centered on the same latitude and longitude (13.1°N , 58.5°E , 50×50 km² identified as “50 km” and 25×25 km² identified as “25 km”). Unless otherwise mentioned, the results are presented for the default domain of 100×100 km² identified as “100 km”.

To analyze the vertical momentum transport, the anomalous vertical flux of zonal ($\overline{u'w'}$) and meridional ($\overline{v'w'}$) momentum was computed following standard Reynolds decomposition. Unless specified otherwise, quantities presented are averaged over the simulation period (except spin-up) and averaged over the domain.

2.1.1. Simulated Convective Regime

The ICON-LEM simulations are dominated by the shallow convective systems over the Atlantic trade wind region as observed during the NARVAL-I campaign (Stevens et al., 2019). In these simulations, organized shallow convective systems typically propagate along the north-easterlies. They occur in various spatio-temporal scales and geometries, although we did not attempt to assign them to a particular group of organi-

zation (either classically well studied “Cloud streets” or recently identified “Fish”, “Flower”, “Gravel”, or “Sugar”) in these simulations (Figure 8). We also noticed a significant amount of gravity waves propagating across the domain.

Here, we do not aim to identify organized systems and associated momentum transport but instead focus on explaining the domain averaged momentum transport which we hypothesize to be a net effect of organized convection, gravity waves, and unorganized turbulent transport.

2.2. BOMEX and RICO Simulations Using DALES

In addition to the aforementioned ICON-LEM simulations, the Dutch Atmospheric Large Eddy Simulation (DALES) model (Heus et al., 2010) was used to simulate the shallow convective cases from BOMEX (Siebesma et al., 2003) and RICO (VanZanten et al., 2011). This model has a horizontal domain size of $12.8 \times 12.8 \text{ km}^2$ with 512 grid points in each direction and 12.5 m resolution in vertical with 224 levels. A second-order advection scheme was used and the sub-grid eddy diffusivities were calculated by a prognostic turbulent kinetic energy (TKE) scheme. The simulations were run for 8 h and the first couple of hours were rejected from the analysis as a spin-up. More details about these simulations can be found in (de Roode et al., 2012).

2.3. Terminology

2.3.1. Apparent Friction

When the total vertical flux convergence ($-\frac{\partial(\overline{u'w'})}{\partial z}$) acts to decelerate the domain mean (also referred to as “background”) winds, we refer to it as apparent friction. Here, the sign of vertical flux convergence tendency is opposite to that of domain mean winds. For the typical trade wind profile (see more discussion later in Section 3) with $u < 0$, positive values of the tendency ($-\frac{\partial(\overline{u'w'})}{\partial z} > 0$) indicate apparent friction.

In the description of results, we simply refer to “apparent friction” as “friction” while keeping in mind that this is an effect on the surrounding flow due to turbulent mixing at smaller scales and not due to relative motion between two surfaces.

2.3.2. Counter-Gradient Fluxes

When the sign of vertical momentum flux is similar to the sign of domain mean vertical wind shear, we refer to it as counter-gradient flux. For example, a counter-gradient zonal flux layer is identified where $\frac{\overline{u'w'}}{u} \frac{\partial \overline{u}}{\partial z} > 0$. In contrast, the down-gradient flux layer has $\frac{\overline{u'w'}}{u} \frac{\partial \overline{u}}{\partial z} < 0$. A similar definition was adapted in past studies (e.g., Larson et al., 2019).

3. Results

3.1. Counter-Gradient Momentum Transport

The tropical wind profile during boreal winters is typically characterized by north-easterly trade winds in the boundary layer that turn to become westerlies somewhere in the free troposphere. There is negative (backward) shear ($\frac{\partial \overline{u}}{\partial z} > 0$) in these winds which can be explained through the thermal wind equation, given the negative meridional temperature gradients. The mean zonal winds during the 8 days of ICON-LEM simulations during December 2013 are consistent with this picture (Figure 1a), except for stronger near-surface easterly winds compared to the climatology ($\sim -7 \text{ m/s}$; Brueck et al., 2015). The mean zonal wind profile shows a jet with an extremum of -14 m/s at 1 km altitude which is about 500 m above the mixed layer top and the mean cloud base height (Figure 1d). Because winds near the surface are slowed down, the

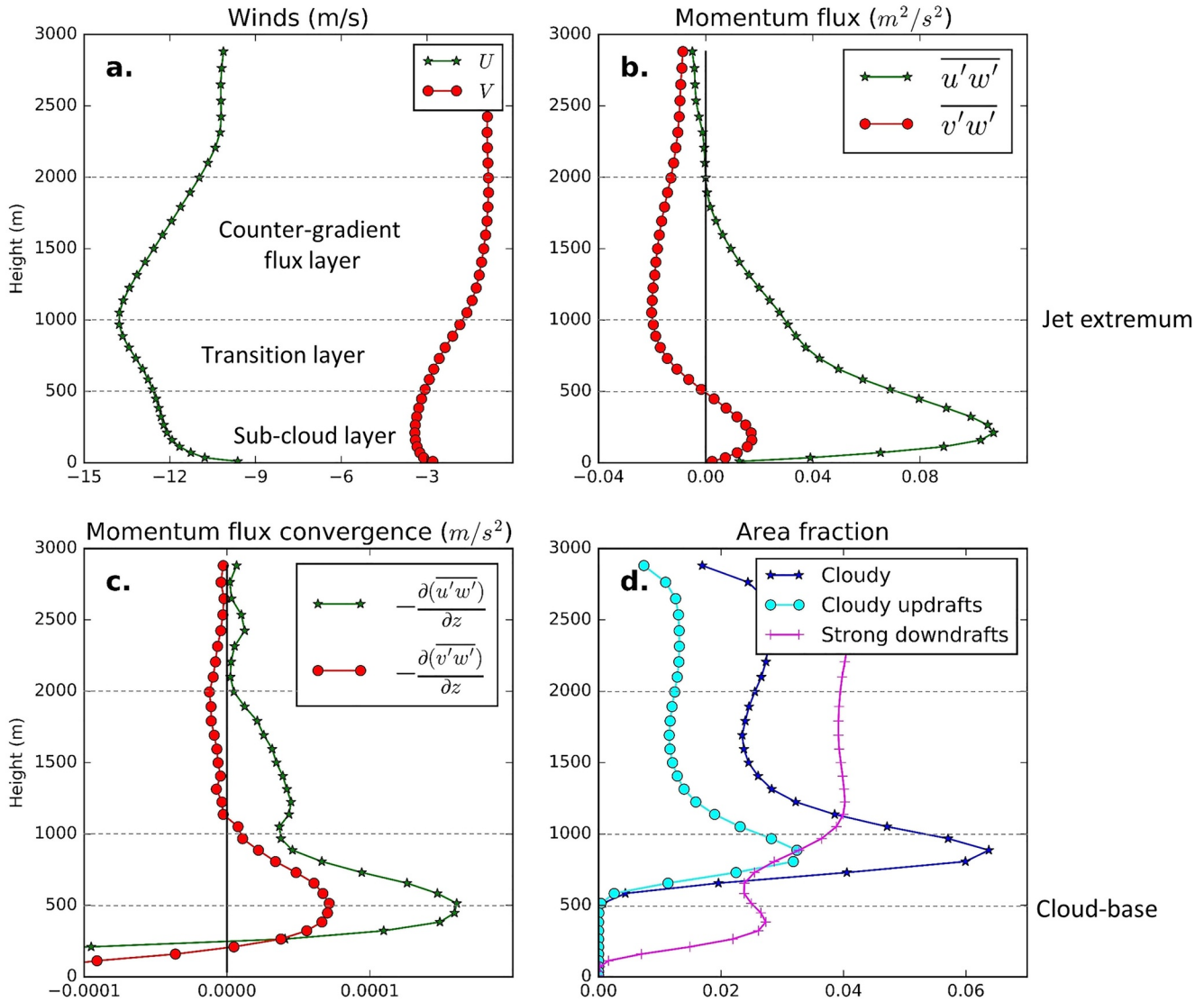


Figure 1. The domain averaged vertical profiles of, (a) zonal (green) and meridional (red) winds (m s^{-1}), (b) zonal (green) and meridional (red) component of vertical momentum flux ($\text{m}^2 \text{s}^{-2}$), (c) zonal (green) and meridional (red) vertical flux convergence tendency (m s^{-2}) and (d) fraction of area covered by Cloudy region (blue), Cloudy updrafts (cyan) and Strong downdrafts (magenta). More details about the identification method for the convective entities can be found in Section 3.4. All values were averaged over the length of ICON-LEM simulation, see details in Section 2.1.

jet introduces a change in vertical shear in the mean profile. The shear is negative ($\frac{\partial \bar{u}}{\partial z} < 0$) below the jet extremum and turns positive ($\frac{\partial \bar{u}}{\partial z} > 0$) above the jet extremum at around 1 km from the surface.

To analyze the role of momentum transport in setting this wind profile, we look at the zonal component of momentum flux ($\overline{u'w'}$). The flux is positive near the surface consistent with the positive surface stress imparted by the ground on the easterly winds. As the turbulent fluxes in the near-surface layer were not available in the output, we analyzed only the “resolved” fluxes at a resolution of 150 m (referred to as fluxes here-onwards). It can be safely assumed that the zonal momentum flux smoothly increases to the near-surface value by the unresolved turbulent fluxes consistent with Helfer et al. (2021). The zonal flux maximizes at around 250 m and smoothly reduces to zero near 2 km above which the flux is small. The flux is down-gradient below the jet extremum as the flux acts to diffuse the mean wind shear, while it is counter-gradient above the jet extremum from 1 km until 2 km. Analysis of time series of momentum flux (not shown) suggests that the counter-gradient momentum flux is an ubiquitous feature in these simulations.

These features are consistent with the recent study by Larson et al. (2019) who found counter-gradient momentum transport in a thin layer (250 m layer) near the jet-extremum in their simulation. In our simulations, the counter-gradient transport occurs over a significantly thicker layer (1,000 m) penetrating all the way until 2 km. Interestingly, other past studies using LES (e.g., Brown, 1999), have not reported significant counter-gradient transport of momentum. These are discussed later in Section 4.

3.2. Friction

The decreasing positive zonal momentum flux introduces a friction on the mean winds (Figures 1b and 1c). In the layer below 500 m where clouds are absent (Figure 1d), the friction mainly occurs through the unsaturated thermals. Disregarding unresolved turbulence below 250 m, the peak in the friction effect through CMT occurs at the base of the transition layer where clouds start to form, at around 500 m. The cloud fraction peaks near 800 m, where the friction effects are minimum and are around 25% of their value just below the cloud base (500 m). In the counter-gradient flux layer above 1 km, the friction effects moderately increase and diminish at around 2 km consistent with the diminishing constant momentum flux at that altitude. In this sense, the CMT acts as a strong friction only below the bulk of the cloud base, is minimum near peak cloud and is moderate near cloud-tops. Hence the notion of “cumulus friction” driven by clouds is contrary to expectation in these shallow convective cases.

It is instructive to discuss the frictional effect in light of previous LES studies. Brown (1999) and Helfer et al. (2020) analyzed the effect of mean shear on convection using LES of marine cumulus convection. Amongst many cases of forward and backward shear they analyzed, they did not report any counter-gradient momentum flux in their simulations. They found friction through CMT in the lower and middle cloud layer. In the top layer, the effect of imposed shear was most pronounced. Only the forward shear ($\frac{\partial \bar{u}}{\partial z} < 0$) case showed friction near cloud tops while the backward shear ($\frac{\partial \bar{u}}{\partial z} > 0$) case indicated wind enhancement through CMT. Zhu (2015) and Schlemmer et al. (2017) mainly analyzed backward shear cases and found friction in the cloud layer only near the jet extremum. As pointed out by Larson et al. (2019), Schlemmer et al. (2017) also simulated a small counter-gradient flux in the cloud layer, but did not discuss it in detail. The same is true for Brown (1999) and Helfer et al. (2020). It is clear from the above discussion that different LES simulations seem to suggest different conclusions about the presence of counter-gradient flux and friction through CMT.

To facilitate the direct comparison, we compared ICON-LEM simulations with the BOMEX/RICO shallow convective cases simulated with the DALES model. Both RICO and BOMEX simulations were forced with similar mean winds (Figure 2b) and produced strong friction near cloud base and counter-gradient momentum flux in a relatively thin layer near the jet extremum (Figure 2a). At the jet extremum, the momentum fluxes are roughly $0.01 \text{ m}^2 \text{ s}^{-2}$, which is a sixth of their peak values of roughly $0.06 \text{ m}^2 \text{ s}^{-2}$ near 100 m from the surface. In comparison, about twice as much flux is present near and above the jet extremum in the ICON-LEM simulations, where the flux near the extremum (1,000 m) is about $0.03 \text{ m}^2 \text{ s}^{-2}$, which is closer to a third of its peak value of $0.11 \text{ m}^2 \text{ s}^{-2}$ near 200 m.

The ICON-LEM simulations clearly have more surface momentum flux than RICO/BOMEX due to stronger mean winds, but they also have a larger fraction of the surface momentum flux that is still present at the base of the cloud layer than in the RICO/BOMEX simulations. More vigorous convection in the ICON-LEM simulations could be responsible for this, but evidently the ICON-LEM simulations also have much more wind shear below and above the jet extremum. Hence, we would also expect a larger influence of local mixing producing negative (down-gradient) momentum fluxes in the lower cloud layer. To disentangle the effects of convection from the wind-shear in the momentum flux production, we next analyze these processes in detail.

3.3. Budget of Momentum flux

The contribution of different processes in producing momentum flux can be analyzed effectively by calculating the budget of the momentum flux. We calculate the momentum flux budget following LeMoine (1983). The budget for the zonal component of vertical flux ($\overline{u'w'}$) can be written as,

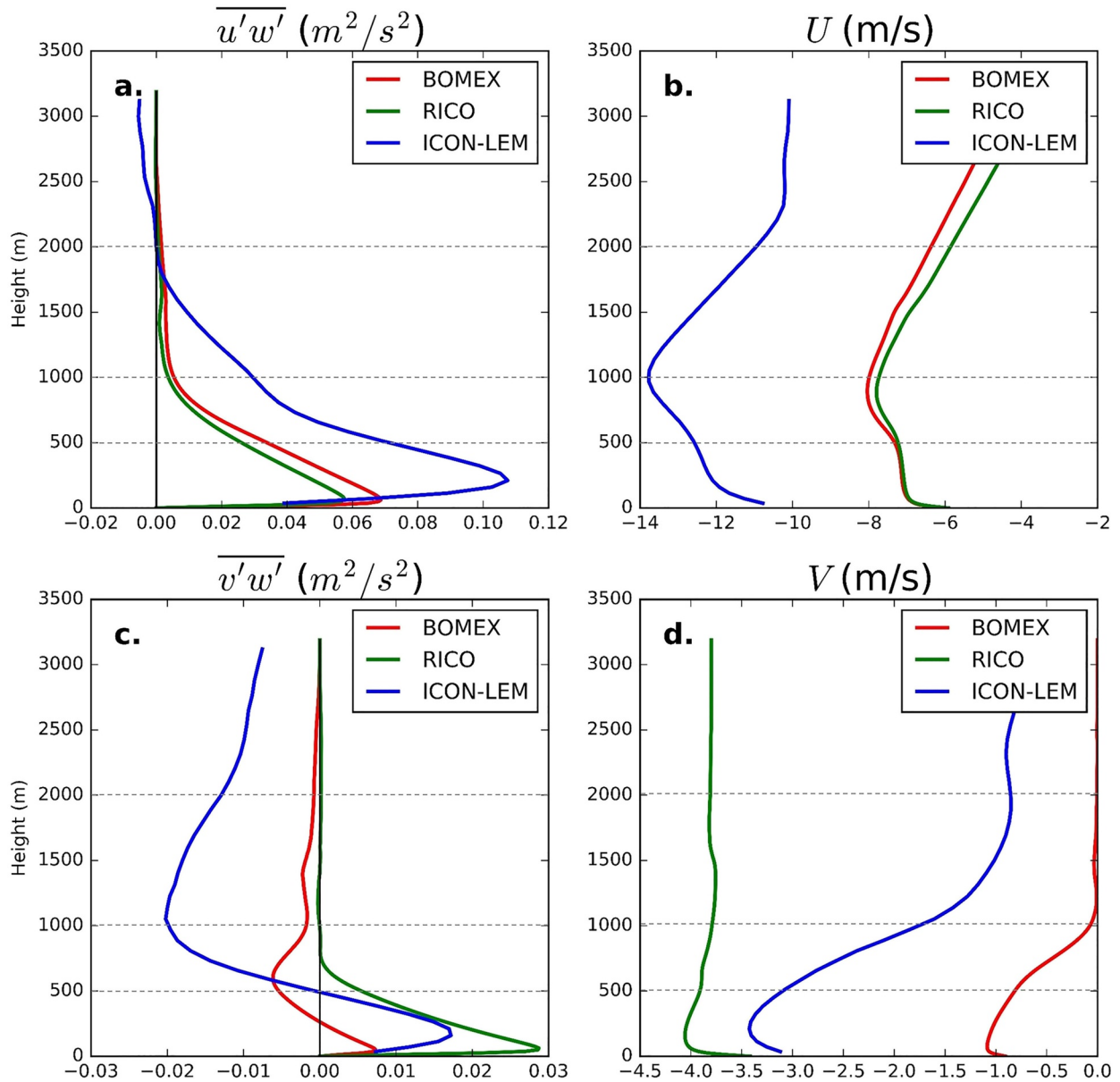


Figure 2. Comparison of domain averaged vertical profiles simulated in BOMEX (red), RICO (green), and ICON-LEM (blue) shallow convective cases. (a) Zonal component of vertical momentum flux (m² s⁻²), (b) zonal winds (m s⁻¹), (c) meridional component of vertical momentum flux (m² s⁻²) and (d) meridional winds (m s⁻¹). All values were averaged over the length of simulation, see details in Section 2.1.

$$\frac{\partial \overline{(u'w')}}{\partial t} = -\overline{w'^2} \frac{\partial \overline{U}}{\partial z} - \frac{1}{\overline{\rho}} \frac{\partial (\overline{\rho u'w'^2})}{\partial z} + \frac{g}{T_v} \overline{u'T'_v} - \left(\frac{w'}{\overline{\rho}} \frac{\partial p'}{\partial x} + \frac{u'}{\overline{\rho}} \frac{\partial p'}{\partial z} \right) + f v'w' + H.trans. \quad (1)$$

where we have used traditional Reynolds decomposition to calculate the mean and perturbation quantities for all fields. The usual symbols following LeMone (1983) are used to designate different terms. While shear production ($S = -\overline{w'^2} \frac{\partial \overline{U}}{\partial z}$), vertical transport ($Tr = -\frac{1}{\overline{\rho}} \frac{\partial (\overline{\rho u'w'^2})}{\partial z}$), buoyancy ($B = +\frac{g}{T_v} \overline{u'T'_v}$) and pressure terms ($HP = -\frac{w'}{\overline{\rho}} \frac{\partial p'}{\partial x}$, $VP = \frac{u'}{\overline{\rho}} \frac{\partial p'}{\partial z}$) were calculated explicitly using the 3D fields available, the effect of horizontal flux convergence (Horizontal transport, “H.Trans.”) is calculated as a residue so as to close the

budget assuming a steady state for the fluxes ($\frac{\partial \overline{u'w'}}{\partial t} = 0$). To test this, we calculated the temporal tendency of the flux with 15 min output (Figure S1). The temporal tendency was found to be significantly smaller than all other terms over a 100 km domain. It is comparable to the small H.Trans term over a 25 and 50 km domain. We expect that the instantaneous tendencies would be even smaller than those calculated with 15 min output. This justifies our assumption of negligible temporal tendencies.

A brief description of terms contributing to the Horizontal transport is provided in Appendix A. The Coriolis terms ($C = f\overline{v'w'}$) arise due to action of the Coriolis force on the meridional component of vertical momentum flux. All gradients were calculated using a finite difference scheme. A vertical profile of the density was available and was used in the calculation of profiles of momentum flux budget terms.

Our main goal is to identify the mechanism that induces a positive momentum flux generation tendency in the counter-gradient layer, but we also use this framework to analyze tendencies in the other layers. We first describe the physical processes associated with each of the terms. The diffusive effect of background wind shear on the momentum flux is captured in the S term. This term is representative of down-gradient diffusion acting through the local wind gradients, which would generate negative momentum flux when vertical wind gradients are positive. This term hence cannot explain the counter-gradient fluxes. The negative tendencies through the diffusive S term need to be compensated by one or a set of other terms to induce a positive momentum flux tendency.

Among other terms, the Tr term signifies the transport which redistributes momentum flux vertically. This term is neither a sink nor a source when considered over the whole convective column. The B term shows the effect of correlated changes in wind and buoyancy perturbation in flux generation. The HP and VP terms show the effect of horizontal and vertical pressure gradients on the flux generation while the HTrans term mainly signifies the effect of horizontal circulations in vertical flux generation. The Coriolis force term is significantly smaller than the other terms and is not shown.

In past studies, it was generally assumed that the effect of horizontal perturbation pressure gradients is mainly to bring the flow back to isotropy. This would happen when the horizontal pressure gradients act to reduce horizontal density gradients. While this is very likely true in the mixed layer on account of isotropic turbulence, it is less likely to be true in the cloud layer where asymmetric horizontal circulations emerge surrounding the clouds. Some previous investigators have found a very important role of horizontal pressure gradients in sheared environments (e.g., Rotunno & Klemp, 1982; Wu & Yanai, 1994). With this background, we explicitly evaluate this term in our simulations.

Similarly, in past studies, the effect of vertical perturbation pressure gradients is assumed to reduce the buoyancy. This stems from the finding that the dominant balance in the vertical momentum budget is between vertical advection, pressure gradients, and buoyancy, with a much smaller role for lateral entrainment of mixing (de Roode et al., 2012). There is a significant body of literature discussing the validity of this assumption (e.g., Houze Jr, 2014; de Roode et al., 2012). We explicitly calculate the vertical perturbation pressure gradient as well.

3.3.1. Hydrostatic Balance on Mesoscales

The dominant balance affecting the momentum fluxes in ICON-LEM is that between the buoyancy term and the vertical pressure gradient term (Figure 3b), in essence establishing hydrostatic balance. The buoyancy term is positive below the cloud layer accounting for the momentum carried by unsaturated boundary layer thermals. This term turns negative near cloud-base, where instead a vertical pressure gradient leads to positive momentum fluxes. In the main cloud layer where effects of latent heating create positively buoyant updrafts again, the buoyancy term turns positive (note that this is also in the counter-gradient momentum flux layer), and the B term peaks just above 2 km where momentum fluxes are small. The momentum flux is thus mainly controlled by the close balance between the buoyancy term (B) and the vertical pressure gradient term (VP).

$$\frac{g}{T_v} \overline{u'T'_v} \sim \frac{u'}{\bar{\rho}} \frac{\partial p'}{\partial z} \quad (2)$$

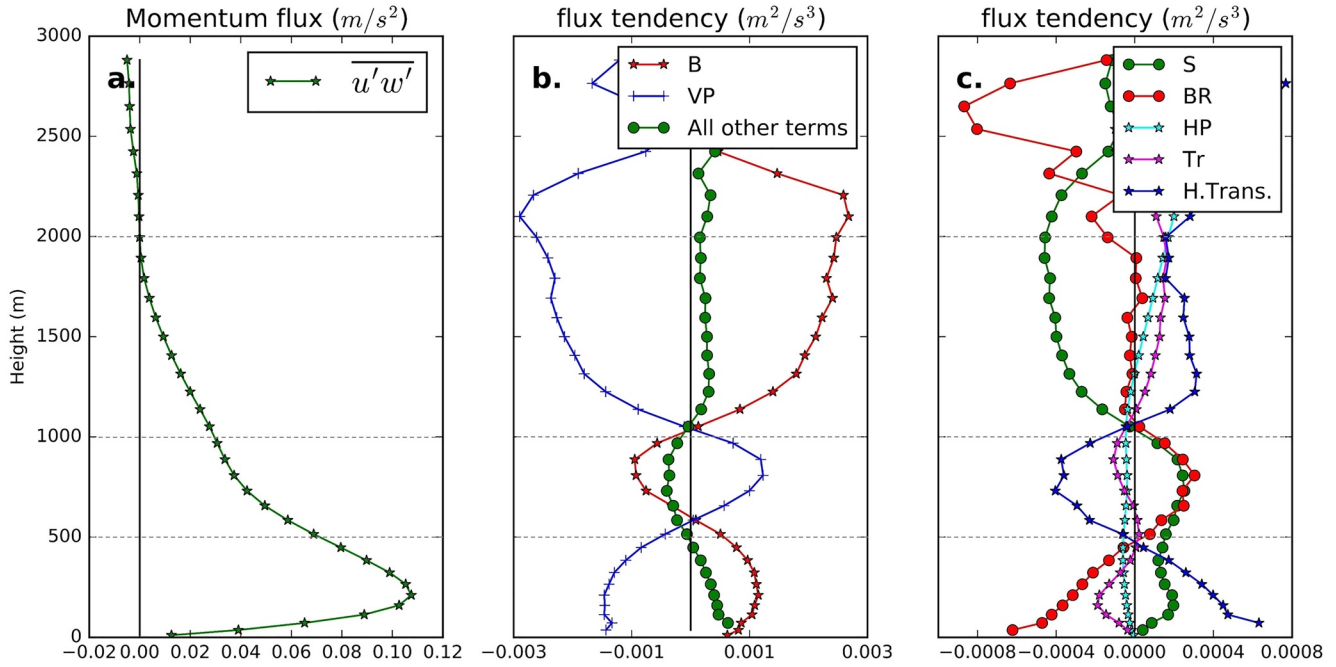


Figure 3. The domain averaged vertical profiles of (a) zonal component of vertical momentum flux ($m^2 s^{-2}$), (b) flux tendency due to Buoyancy term B (red), vertical pressure gradient term VP (blue), and sum of all other terms in the zonal momentum flux budget (green) (All in $m^2 s^{-3}$, see Equation 1) and (c) flux tendency due to individual terms (shear driven turbulence term S (green), vertical transport term Tr (magenta), horizontal pressure term HP (cyan)) in the budget when compared to the buoyancy residue (BR, red) and horizontal transports HTrans (blue) ($m^2 s^{-2}$). See the text for definitions.

Numerous authors studying vertical velocity of updrafts have indeed suggested that rather than looking at absolute buoyancy, buoyancy should be interpreted as the “statically forced part of the locally non-hydrostatic, upward pressure gradient force” in other words, an “effective buoyancy” equivalent to the sum of absolute buoyancy and the vertically oriented buoyancy pressure gradient force (see the discussion in Peters [2016] and also Doswell and Markowski [2004] and Romps and Charn [2015]).

To find out what really drives differences in momentum fluxes, we should compare the small residue between the pressure and buoyancy term (which is a result of the nonhydrostatic pressure perturbations) with the other terms in the budget to draw a comparison. In the flux budget we study here, we define the buoyancy residue (BR) as:

$$BR = \frac{g}{T_v} \overline{u'T'_v} - \frac{u'}{\bar{\rho}} \frac{\partial p'}{\partial z} \quad (3)$$

The BR is positive in the transition layer near the cloud base. In the sub-cloud and transition layer, shear also helps to generate a positive flux. In the counter-gradient flux layer on the other hand, the BR is essentially zero (Figure 3c). In the counter-gradient flux layer, shear instead plays an important role in diffusing the momentum flux, while the horizontal transport term and horizontal pressure gradients act to enlarge a positive (thus counter-gradient) momentum flux. The most dominant term inducing the positive flux tendency in the counter-gradient flux layer is the momentum transport through horizontal circulations. The flux transport through horizontal circulations is also significant in the sub-cloud layer below 500 m signifying that the resolved scale circulations (such as cold-pool driven gust fronts) also significantly influence flux generation in this layer.

These results are notably different from recent LES simulations by Larson et al. (2019). They found that the dominant balance in their simulations was between the buoyancy term, the vertical transport term, and the vertical shear term. The buoyancy and transport terms induced the positive (thus counter-gradient) flux in their simulations, while the vertical shear diffused them. In contrast, in the present simulations, the domain averaged zeroth-order balance is between vertical pressure gradient and buoyancy term, which signifies a

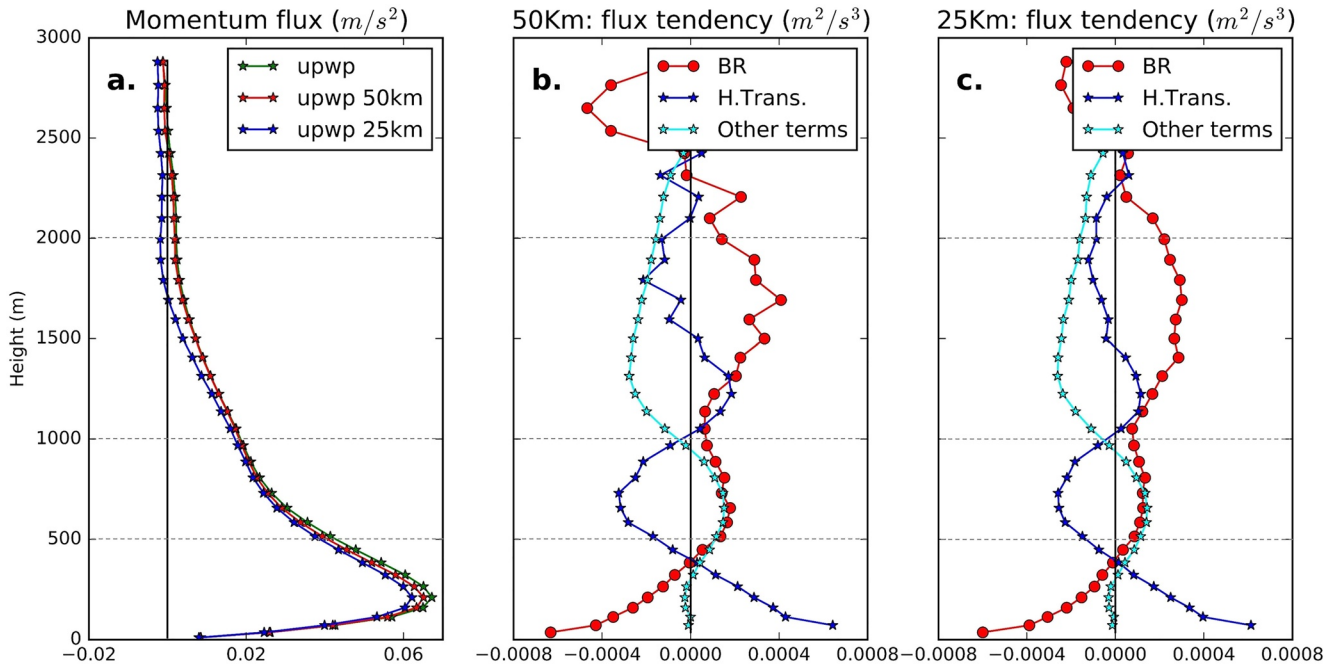


Figure 4. The domain dependence of zonal momentum flux ($m^2 s^{-2}$) (a) and the budget terms in Equation 4: BR (red), H Trans (Blue), and Other terms (Cyan) in 50 km (b) and 25 km (c) domain sampling ($m^2 s^{-3}$).

hydrostatic balance (Equation 2). The first order balance driving the tendency of momentum flux is dominated by the flux transport through horizontal circulations ($H.Trans \gg BR$).

In conclusion, the horizontal circulations primarily drive positive counter-gradient momentum flux tendency while vertical transport and horizontal pressure terms lead to small increases in the flux. The (large) shear overall reduces the momentum fluxes through turbulent diffusion.

3.3.2. Domain Size Dependence

One potential reason for the different momentum flux in the ICON-LEM simulations compared to those discussed by Larson et al. (2019) is that the domain in the present case ($100 \times 100 km^2$) is significantly larger than the one in Larson et al. (2019) ($25 \times 25 km^2$). We chose this domain to ultimately derive statistics suitable for improving the convective parameterizations in climate models. To test the effect of domain size, we repeated the budget calculation over smaller subsets of our domain. Figure 4 shows a simplified form of the momentum flux budget,

$$BR + HTrans + (S + Tr + HP) = 0 \quad (4)$$

where $(S + Tr + HP)$ are referred as “Other terms”. When Sampled over 50 km, the zeroth-order balance is hydrostatic; similar to the one in the 100 km, except that the buoyancy residue (BR term) is non-negligible in the counter-gradient flux layer (Figure 4b). The vertical transport and horizontal pressure terms are similar as in the 100 km domain (not shown explicitly) but the effect of horizontal circulations is smaller.

A similar picture is seen in the 25 km domain with even a larger buoyancy residue (BR) indicating significant nonhydrostatic pressure perturbations (Figure 4c). When sampled over comparably smaller domains; the first order balance becomes similar to the one observed by Larson et al. (2019) for RICO. Remember that zeroth-order balance is still significantly different from Larson et al. (2019). To test if our results are sensitive to the placement of smaller domains within 100 km domain, we repeated this analysis in four sets by placing the center of 25 and 50 km domain either close to or far away from the lateral boundaries (Figures S2 and S3). The results were found to be insensitive to the exact placement.

It is clear from this analysis that positive momentum flux tendency is mainly induced by the buoyancy term at cloud cluster scale ($\sim 25 km$) but is mediated by associated horizontal circulations when considered over

a larger domain (~100 km). This is expected to have significant implications for the CMT parameterizations and the so-called top-hat (or bulk plume) approximation. This approximation assumes that a significant transport of a quantity occurs mainly through strong updrafts and downdrafts while the rest of the turbulent flow accomplishes relatively smaller transports. This is an excellent approximation for the heat or scalar transport (Siebesma & Cuijpers, 1995) as these properties are mostly confined to the convecting entities (like updrafts and downdrafts, etc.) but momentum transport, in contrast, is also altered by the pressure gradients that drive horizontal circulations on larger areas, where the existence of the latter depends on the simulation domain.

3.4. Transport Through Clouds

To evaluate what part of the total momentum and momentum flux is actually carried through different convecting entities, we applied the following objective-based definitions to identify them in the 3D ICON-LEM fields,

1. Cloudy: refers to average over all grid-points with positive cloud liquid water ($cld > 0$).
2. Updrafts: refers to average over all grid-points with positive vertical velocity ($w > 0$, which can locate in the cloud or sub-cloud layer).
3. Cloudy updrafts: refers to average over all cloudy grid-points with positive velocity ($w > 0$ and $cld > 0$).
4. Strong downdrafts: refers to average over all grid-points with stronger than 0.5 m s^{-1} negative vertical velocity ($w < -0.5 \text{ m s}^{-1}$).

3.4.1. Momentum Transport

In the cloud layer above 500 m, the cloudy updrafts have significantly slower zonal speeds as compared to their environments inducing a cumulus friction (Figure 5a). Above 1,500 m, the cloudy updrafts have faster speeds than the environmental wind. The unsaturated updrafts below the cloud base have slightly slower speeds. The strong downdrafts have similar speeds as the environment except in two layers: (1) In the sub-cloud layer, the downdrafts move at significantly faster speeds inducing friction on the background flow. This is likely an effect of asymmetric cold-pools, as symmetric cold pools are less likely to have any domain mean net influence. (2) In the layer between 1,500 and 2,500 m, the strong downdrafts have slightly faster horizontal speeds inducing weak friction.

In the meridional direction, the cloudy updrafts have faster speeds than the environmental wind (opposite to “cumulus friction”) while the downdrafts fall at similar speeds inducing negligible effect (Figure 5b). The updrafts below the cloud base have slower speeds than the environment contributing to friction on the background flow.

3.4.2. Momentum Flux Transport

The cloudy updrafts have a non-monotonic momentum flux profile (Figure 5c). Their momentum flux increases starting from low values near cloud base to significantly larger values near the jet extremum at 1,000 m. In this layer, the flux convergence of the cloudy updraft flux suggests a significant reduction in the cumulus friction. In fact, in this layer, the contribution from cloudy updrafts is to enhance (opposite to the notion of “cumulus friction”) the winds below the jet extremum. This is consistent with the sharp decrease in cumulus friction effect near the cloud fraction maximum discussed before (Figure 1). Above the altitude of the jet extremum at 1 km, the flux through cloudy updrafts sharply turns negative indicating no contribution to the counter-gradient (positive) momentum flux through cloudy updrafts above 1.3–1.5 km. This is consistent with the findings from the momentum flux budget that the buoyancy residue (BR) is approximately zero above 1 km (Figure 3).

The clouds (cloudy samples) carry at least a 3–4 times larger positive momentum flux in the lower part of the counter-gradient flux layer, but sharply turn negative at around 1,500 m consistent with their speeds, suggesting lack of cloudy contributions to the counter-gradient flux above 1,300 m up to 2,000 m (Figure 5c). The strong downdrafts carry a significant positive momentum flux in the mixed layer below 500 m and near cloud-tops above 1500 m (Figure 5c). This is consistent with their slower speeds than the environment as noticed before (Figure 5a).

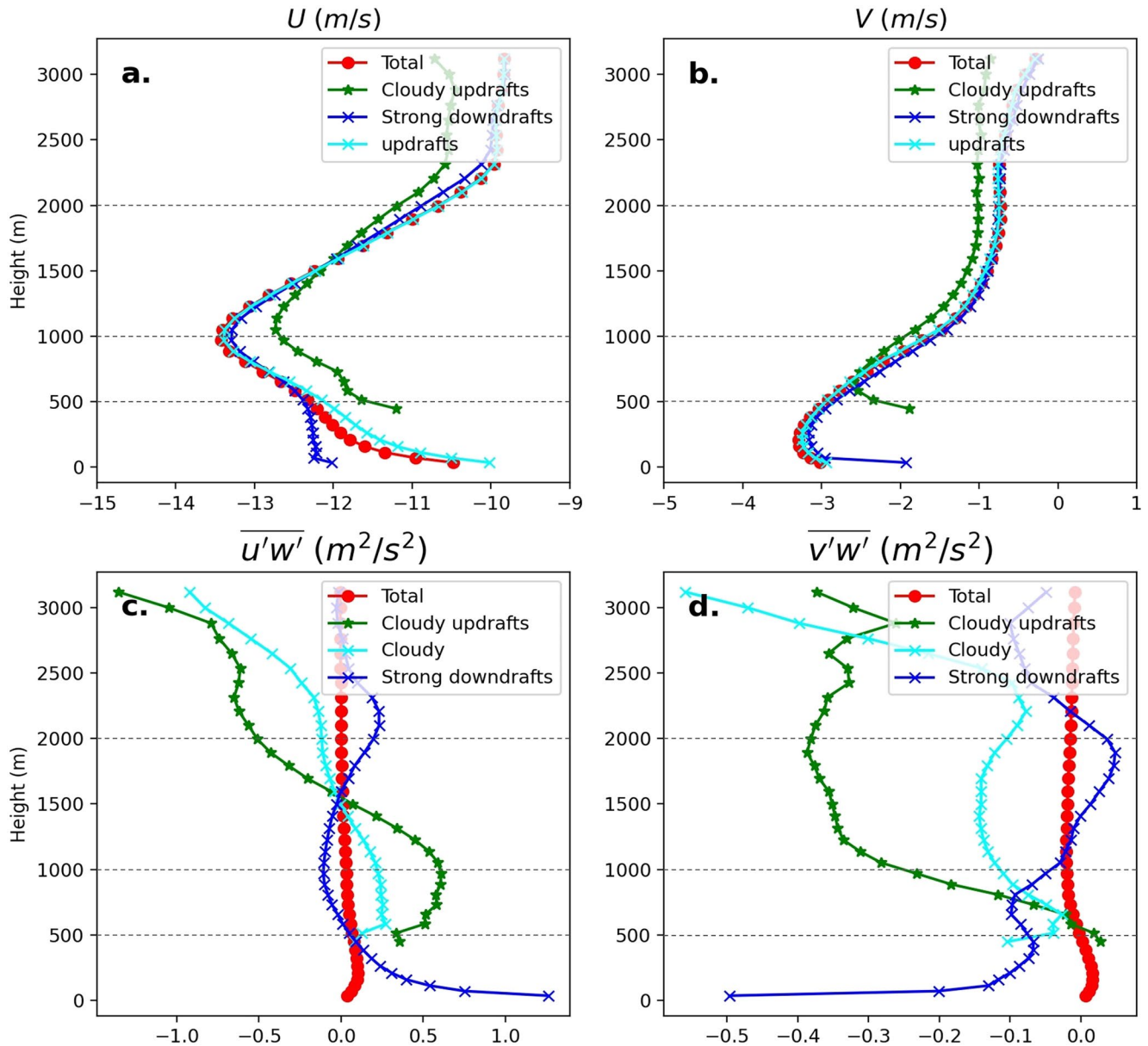


Figure 5. The domain mean vertical profiles of winds and vertical momentum fluxes along with the contributions from Cloudy updrafts and Strong downdrafts (See Section 3.4 for definitions), (a) zonal wind (m s^{-1}), (b) meridional wind (m s^{-1}), (c) zonal component of vertical momentum flux ($\text{m}^2 \text{s}^{-2}$), and (d) meridional component of vertical momentum flux ($\text{m}^2 \text{s}^{-2}$).

The meridional momentum flux shows that both clouds and cloudy updrafts carry significant negative flux (Figure 5d). This flux is partly compensated by the environmental momentum flux (not shown) to ultimately render a weak negative momentum flux profile in the cloud layer (Figure 1).

The consistency between conditionally sampled momentum flux and previously discussed momentum flux budget further bolsters our finding that in the main cloud layer and near cloud tops (between 1 and 2 km), mesoscale horizontal circulations predominantly lead to the transport of extra positive momentum flux.

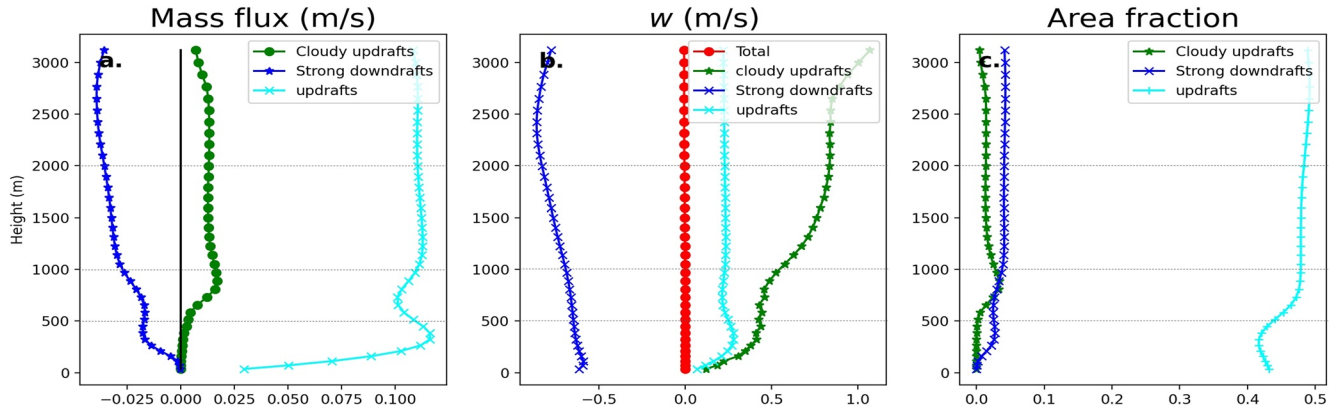


Figure 6. The domain mean vertical profiles of (a) mass flux (m s^{-1}), (b) grid mean w wind (m s^{-1}) and (c) grid mean area fraction through objectively sampled Cloudy updrafts (green), strong downdrafts (blue), and updrafts (cyan).

3.5. Testing Mass-Flux-Based Parameterizations

In some climate models, the shallow CMT is represented by the traditional mass-flux-based parameterizations. It is useful to evaluate if these parameterizations represent the counter-gradient flux contribution near cloud tops and the weak friction effect throughout the cloud layer that we observed in our simulations.

To facilitate the evaluation, we follow Gregory et al.'s (1997) decomposition to calculate the contributions from cloudy updrafts and strong downdrafts to the total momentum flux. Furthermore, we also calculate contributions from updrafts in setting the momentum flux below cloud-base. This later contribution is often not represented in many traditional parameterizations (e.g., Gregory et al., 1997).

$$\overline{u'w'} \sim M_{cu}u'_{cu} + M_d u'_d + M_u u'_u \quad (5)$$

Here, M_{cu} , M_d , and M_u are mass fluxes in the cloudy updrafts, strong downdrafts, and updrafts respectively. They are calculated as a product of vertical velocity and area fraction using objective-based definitions (see Section 3.4). u'_{cu} , u'_d and u'_u are the relative zonal (or meridional) velocities in the cloudy updrafts, strong downdrafts, and updrafts with respect to the background velocity, respectively. Before we evaluate the total contribution to the momentum flux, we first analyze the profiles of mass flux.

3.5.1. Profiles of Mass Flux

The vertical profiles of mass flux have a peculiar vertical structure (Figure 6). The maximum mass flux through updrafts is observed below the cloud base, decreases in the cloud layer and remains constant in the counter-gradient flux layer near cloud-tops (between 1 and 2 km, Figure 6a). The mass flux through strong downdrafts peak near cloud-tops (around 2.5 km) where either the entraining air or subsiding shells likely play an important role (Heus & Jonker, 2008).

We further analyzed the contribution to mass flux from vertical velocity and area fraction of the drafts (Figures 6b and 6c). The updraft velocities peak below cloud base but have relatively smaller area fraction. In comparison, the velocities in cloudy updrafts peak near cloud-tops (near 2 km) but have a maximum area fraction in the transition layer (near peak cloud) at around 800 m. In effect, their net contribution to the mass flux peaks in the transition layer. In contrast, for strong downdrafts, vertical velocities as well as their area fraction both peak near cloud-tops (near 2 km). This further corroborates a possible role of subsiding shells in generating strong mass flux near cloud-tops in these simulations.

3.5.2. Mass Flux-Based Contribution to Momentum Flux

Now we calculate the mass flux-based contribution to the total momentum flux. Consistent with the lack of clouds below 500 m (Figure 1d), the contribution of cloudy updrafts to the total momentum flux is insignificant in the sub-cloud layer (Figure 7a). Near the upper part of the cloud layer (~ 1 km), the cloudy updraft contribution is positive. This cloudy updraft contribution sharply becomes negative at around 1,500 m

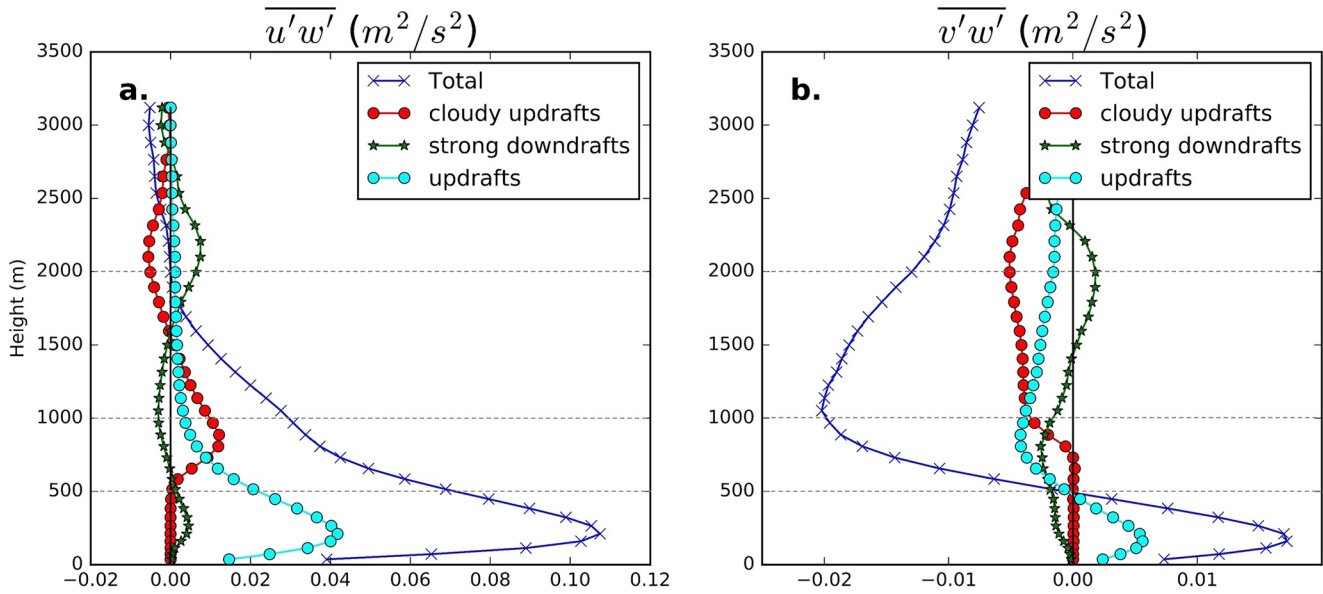


Figure 7. The domain mean vertical profiles of total momentum flux ($\text{m}^2 \text{s}^{-2}$) in ICON-LEM (blue) and total flux carried through objectively sampled Cloudy updrafts (red), strong downdrafts (green), and updrafts (cyan) for (a) zonal component and (b) meridional component.

consistent with faster cloudy updraft speeds noted before (Figure 5c). Below the cloud layer, a significant contribution (around 35% of the total flux) to the flux occurs mainly through the unsaturated updrafts.

Also consistent with Figure 5a, the strong downdrafts induce positive momentum flux below 500 m possibly through asymmetric cold-pools (Figure 7a). The downdrafts have a small negative flux contribution in the cloud layer and in the lower part of counter-gradient flux layer. Interestingly, although the difference between the downdraft velocity and environment was found to be small above 1.5 km (Figure 5a), their net contribution to the momentum flux is significant (Figure 7a). This suggests that contributions to the momentum flux are dominated by the profile of mass flux in strong downdrafts near cloud-tops. In fact, the significant positive contribution from strong downdrafts almost cancels the negative contribution from cloudy updrafts inducing a small flux above 2 km.

A similar picture emerges for the meridional momentum flux (Figure 7b). The cloudy updrafts carry negative momentum flux above the cloud layer. The downdrafts carry negative momentum flux in the transition layer but carry small momentum flux above it.

To conclude, mass-flux-based estimations of the momentum flux capture the right sign of the momentum flux in the transition layer near cloud base but severely underestimate it. The representation of the thick positive counter-gradient flux layer is not captured by the mass-flux-based parameterizations. Furthermore, contributions from unsaturated updrafts are significant below the cloud base and need to be included in the mass-flux-based parameterizations.

3.6. Shallow Convective Organization and Counter-Gradient Momentum Flux Transport

Our analysis of momentum flux budget suggested that the counter-gradient flux transport is orchestrated by the horizontal circulations surrounding the cloud-tops with spatial scales large enough not to be fully captured in small domains. Further analysis confirmed that the momentum flux carried by the objectively sampled cloudy updrafts, downdrafts do not account for the counter-gradient flux. Instead, as suggested in the literature, the gravity waves and different geometries of convective organization may lead to counter-gradient momentum transport (Larson et al., 2019; Moncrieff, 1992).

To visualize the horizontal circulations, their spatial extent, and their relation to shallow convective organization we analyzed maps of zonal momentum flux ($\overline{u'w'}$) and cloud liquid water in the counter-gradient flux layer (Figure 8). The clouds organize in different geometries starting from individual cloud clusters to a

Zonal Momentum Flux (Shade), Clouds (Contours) at 1.5km altitude

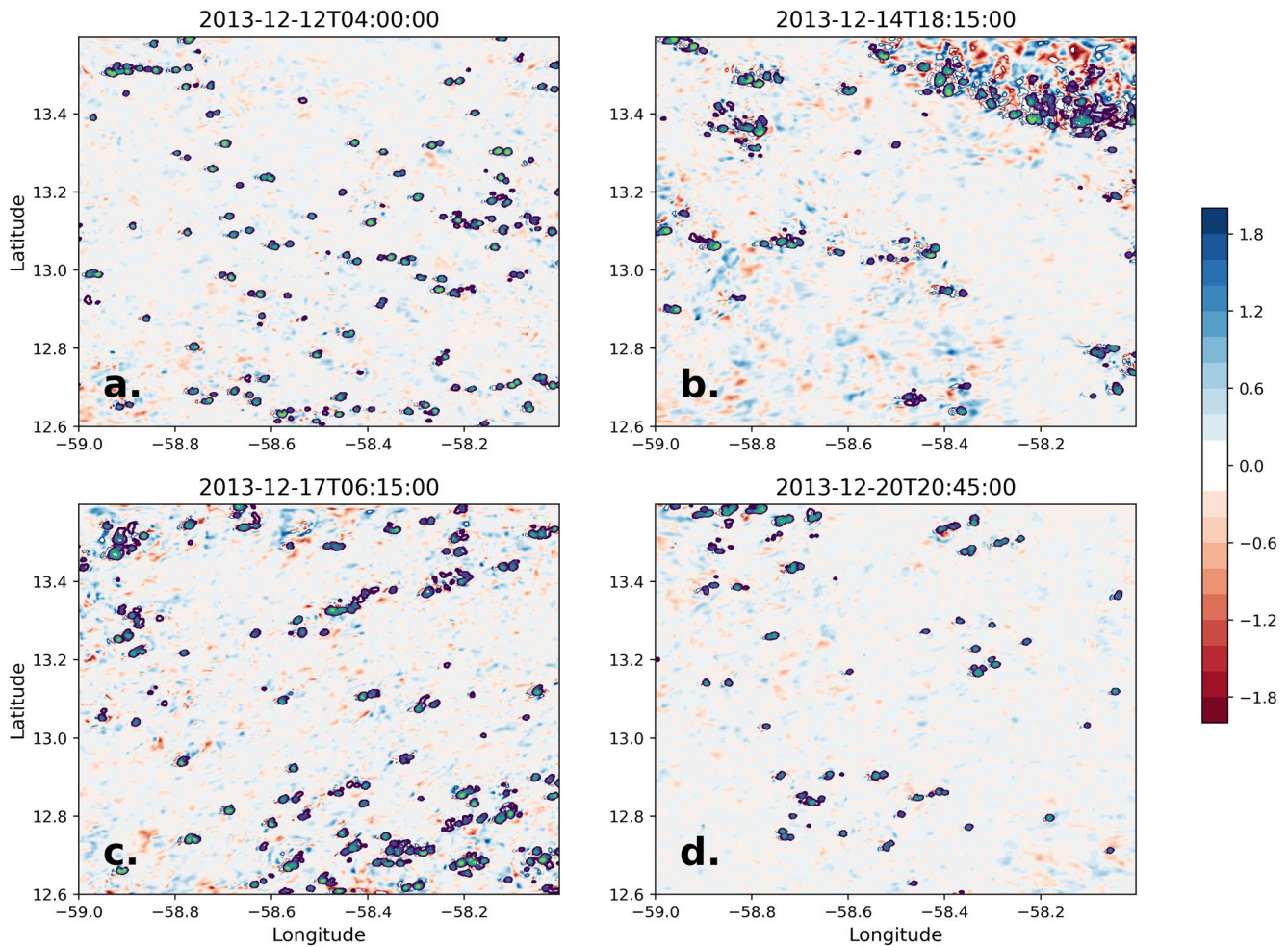


Figure 8. The maps of distribution of zonal momentum flux ($\overline{u'w'}$ $\text{m}^2 \text{s}^{-2}$, shaded) and cloud liquid water (contours with interval 0.5 g kg^{-1}) at four randomly sampled time stamps within the counter-gradient flux layer at 1.5 km altitude.

mesoscale shallow convective system that known to occur in tropical doldrums (Klocke et al., 2017; Stevens et al., 2020). Although, a large positive (counter-gradient) momentum flux typically occurs in the vicinity of a cloud cluster, interestingly a significant momentum flux can be seen as far away as 25 km from the cloud cluster. It is likely that the horizontal circulations triggered by nonhydrostatic pressure gradients quickly carry momentum flux farther away from the cloud cluster (see the animation generated from 15 min output in supporting information S7). This is also observed in the peak cloud layer (Figure S4), where clouds occur more frequently throughout the domain. In the mixed layer below cloud base, the updrafts are seen to be organized in a linear fashion (like cloud streets) although significant momentum flux can be seen farther away from them (Figure S5).

4. Discussion

4.1. Mechanism of Flux Generation

Our analysis of momentum flux budget revealed new processes driving counter-gradient momentum flux near cloud-tops in these simulations as compared to past studies (Larson et al., 2019; Schlemmer et al., 2017). It is worth doing a detailed scrutiny of the physical mechanism controlling these. We begin by

distinguishing the mechanisms that produce positive (counter-gradient) momentum flux and friction, and later discuss how divergent horizontal circulations contribute to flux generation.

As a friction depends on the convergence of momentum flux, the mechanisms that produce positive (and hence counter-gradient) momentum flux act against the friction effect. Hence, these mechanisms weaken the friction in the transition layer and instead distribute it over a thicker layer by weakening the gradients of momentum flux.

The dominant mechanisms of momentum flux generation strongly depend on the relative magnitude of pressure terms, buoyancy terms, and horizontal circulation terms. The importance of these terms depends on the ability of the simulation to generate realistic balances in the vertical momentum equation and correlations of horizontal momentum fluxes with vertical winds. The dominant balance in the vertical momentum equation is not understood completely and is still an active research topic with unresolved paradoxes and enigmas (de Roode et al., 2012; Hernandez-Deckers & Sherwood, 2016; Morrison, 2016; Romps & Charn, 2015; Sherwood et al., 2013).

It is useful to discuss this complexity using an example of a buoyant thermal similar to previous classical studies (e.g., Doswell III & Markowski, 2004; Houze Jr, 2014). A buoyant thermal can rise up pushing away the fluid above it laterally. Consequently, as the thermal rises up other fluid has to occupy its space below to satisfy mass continuity. This implies that high pressure must develop above the thermal and low pressure below it. If this pressure gradient exactly balances the buoyancy force, then during the motion the thermal faces no vertical acceleration. In this situation, significant horizontal accelerations may still get generated (Das, 1979; List & Lozowski, 1970).

In this case, hydrostatic balance is established in the effective area of influence over which the thermal is able to push fluid laterally. If a small area surrounding the thermal is considered then the buoyancy residue (buoyancy force not balanced by vertical pressure gradients) can be large as only a part of the fluid pushed away by the thermal would be under consideration. But if an adequately large area surrounding a thermal is considered then the buoyancy residue is likely to be zero as all the fluid involved in the horizontal mass movement would be accounted for. In that latter case, even though the system would be in hydrostatic balance as a whole, the impact of buoyancy is manifested in terms of the generation of horizontal circulations.

This is likely the case in our 100 km domain where horizontal circulations carry most of the momentum flux divergence. In contrast, on the 25 km domain case, the buoyancy is the dominant term, while horizontal circulations have a small influence. This is expected because when only a limited area around the thermal is considered, the cloud-scale and mesoscale fluctuations of horizontal wind and associated momentum transport are severely underestimated.

Moncrieff (1981, 1992) and Moncrieff et al. (2017) propose that the momentum transport through mesoscale organization of deep convective systems can be successfully parameterized with an archetypal model that considers the cross-cloud pressure gradient and associated circulations. While the nature of counter-gradient transports near cloud tops in our simulations bears similarities with Moncrieff et al. (2017), more analysis is required to systematically derive similarities and differences between transport through shallow and deep convective organization, which is beyond the scope of this work.

4.2. Effect of Model Set-Up

It is likely that a model set-up with double periodic boundary conditions and limited domain size imposes constraints on the development of the horizontal circulations. This is possible because even though the clouds occupy only 4%–6% of the domain area at any point of time, the associated horizontal circulations may sometimes develop over significantly (sometimes 10 times) larger regions on account of strong horizontal accelerations. A model domain only 10 times the size of a cumulus cloud will pose a significant constraint for the development of other adjacent clouds.

The conclusions about the dominant balance in the vertical momentum budget will likely be dependent on the ability of the simulation to resolve surrounding circulations realistically. In this aspect, the present ICON-LEM set-up surpasses earlier investigations as it has a large domain and does not enforce periodic boundary conditions.

5. Conclusions

In this study, we utilized the unique multiday simulations of ICON-LEM at 150 m resolution to investigate the character of shallow CMT over the tropical Atlantic. We analyzed the resolved flows in the boundary layer and the cloud layer to demonstrate that shallow convection acts like an “apparent friction” to decelerate the north-easterly trade winds. The decelerations are strongest just below where most cloud bases reside, at the base of the transition layer (at 500 m from surface), and are orchestrated by unsaturated updrafts. In the peak cloud layer (800 m), the cumulus friction is small but is distributed over a thicker layer than found in earlier investigations.

The distinguishing feature of ICON-LEM simulations is the presence of counter-gradient zonal momentum flux in a 1 km thick layer above the jet extremum (at 1 km) near cloud-tops. The counter-gradient flux layer here is almost twice as thick as those observed in the idealized simulations of BOMEX and RICO.

To understand the mechanism sustaining the counter-gradient momentum flux we calculated the budget of momentum flux. This allowed us to separate the effect of shear-driven turbulence on the momentum flux from the effect of buoyant convection. Detailed analysis of different mechanisms influencing the momentum flux revealed that the dominant mechanism acts through a subtle balance between the flux generation through nonhydrostatic buoyancy residue (BR) and the horizontal circulations triggered by the associated pressure gradients. These mechanisms produce significant positive, counter-gradient momentum flux that counteracts the negative flux production through shear-driven turbulent diffusion near cloud tops. In the sub-cloud layer, the horizontal circulations enhance the down-gradient turbulent diffusion.

The identification of the dominant mechanism was found to be dependent on the domain size and the ability of the model to realistically simulate the horizontal circulations surrounding clouds. Simulations with idealized, doubly periodic boundary conditions are likely to face artificial constraints in simulating these circulations. As ICON-LEM was devoid of these problems; our analysis is qualitatively better than previous estimates, even though further improvement in the resolution would help improve these estimates.

We further analyzed the momentum and momentum flux transport through objectively identified convective entities. Consistent with our previous analysis, we find that clouds impart weak friction as they mix air with slower horizontal speeds with their surroundings. The positive momentum flux carried through clouds quickly diminishes to zero in the upper part of the cloud layer (near 1.5 km). In effect, clouds do not contribute significantly to the counter-gradient momentum flux near cloud-tops.

The momentum transport represented by mass-flux-based parameterizations is found to capture the right sign of the flux in the transition layer (800 m from surface) but underestimates it severely. The unsaturated updrafts are found to carry significant momentum below cloud base (below 500 m) and need to be represented in traditional parameterization. The momentum flux in the counter-gradient layer near cloud tops is not represented by these parameterizations.

The nature of shallow CMT reported here bears remarkable similarities to the momentum transport through well-studied organized mesoscale convective systems. The down-gradient momentum transport in the lower layers and counter-gradient momentum transport near cloud tops reported here have also been observed in deep convective organization (LeMone, 1983; Moncrieff, 1981, 1992). Grubišić and Moncrieff (2000) numerically simulated and modeled CMT by organized shallow convection in cold-air outbreaks behind mid-latitude cyclones in a sheared environment. They demonstrated that CMT was successfully parameterized as a special case of the down-shear tilted dynamical regime of Moncrieff (1978). A possible avenue for future work is to evaluate if parameterizations proposed for the mesoscale systems can be adapted to include purely shallow convective organization.

In conclusion, this study demonstrates that a significant counter-gradient momentum flux remains near cloud-tops due to momentum flux generation by nonhydrostatic pressure gradients and horizontal circulations surrounding them. These new mechanisms of momentum transport are not represented in most climate models and may have fundamental implications for simulations of the trade winds.

Appendix A: Horizontal Transport Terms

The momentum flux budget presented in Equation 1 combines all terms that are not explicitly represented in Horizontal transport (“H. Trans”) term. These consist of four terms,

$$H.Trans = -\bar{U} \frac{\partial \overline{u'w'}}{\partial x} - \frac{\partial \overline{u'^2 w'}}{\partial x} - \left(\overline{w'v} \frac{\partial \overline{u'}}{\partial y} + \overline{u'v} \frac{\partial \overline{w'}}{\partial y} \right) - \frac{1}{\bar{\rho}} \frac{\partial (\bar{w} \overline{\rho u'w'})}{\partial z} \quad (A1)$$

The first term on the right-hand side represents the zonal flux convergence through mean zonal winds, the second one represents the zonal flux convergence through perturbation winds, the third term is similar to the first two but for flux convergence in the meridional direction. The last term represents the vertical flux convergence through mean vertical winds.

The vertical convergence term is likely to be smallest on account of small domain mean vertical winds both in 25 or 100 km, also consistent with findings of LeMone (1983). Then the resultant transport is dominated by flux convergence in zonal and meridional directions. We call it “Horizontal transport” for simplicity keeping in mind that it occurs mainly through horizontal flux convergence.

Here, it is important to highlight the difference between the momentum *flux* budget and the momentum budget. In the momentum budget, the domain averaged flux divergence terms such as $\frac{\partial \overline{u'u'}}{\partial x}$ and $\frac{\partial \overline{u'v'}}{\partial y}$ are equal to the difference between momentum fluxes entering and leaving the lateral boundaries following Gauss’s divergence theorem and are generally small. The same is not true for the momentum *flux* budget presented here in Equations 1 and A1. Here terms such as $w' \frac{\partial \overline{u'v'}}{\partial y}$ appear and they do not necessarily average to zero.

Data Availability Statement

The authors thank German HD(CP)² project team and DKRZ for conducting the simulations and making ICON-LEM data available. The DALES simulations were kindly provided by Stephan de Roode. The ICON-LEM data are stored at German Climate Computing Centre and are available through Stevens et al. (2019) and Klocke et al. (2017); while the DALES simulations are available through de Roode et al. (2012). Technical help from Erwin and Anuja in the initial phase of the project is appreciated.

Acknowledgments

This study was supported by “Cloud-Break” project funded by the European Research Council (ERC) under the European Union’s Horizon 2020 Research and Innovation Program (Starting Grant Agreement No. 714918). Vishal Dixit was benefited by scientific discussions with Cathy Hohennegar, Stephan de Roode, Pier Siebesma, Mariska Koning, Beatrice Saggiorato, and Niranjan G. The authors thank Dr. M Moncrieff and an anonymous reviewer for their constructive comments which lead to significant improvement in the analysis and presentation of this study.

References

- Badlan, R. L., Lane, T. P., Moncrieff, M. W., & Jakob, C. (2017). Insights into convective momentum transport and its parametrization from idealized simulations of organized convection. *Quarterly Journal of the Royal Meteorological Society*, 143(708), 2687–2702. <https://doi.org/10.1002/qj.3118>
- Bony, S., Schulz, H., Vial, J., & Stevens, B. (2020). Sugar, gravel, fish, and flowers: Dependence of mesoscale patterns of trade-wind clouds on environmental conditions. *Geophysical Research Letters*, 47(7), e2019GL085988. <https://doi.org/10.1029/2019gl085988>
- Bony, S., Stevens, B., Frierson, D. M. W., Jakob, C., Kageyama, M., Pincus, R., et al. (2015). Clouds, circulation and climate sensitivity. *Nature Geoscience*, 8(4), 261–268. <https://doi.org/10.1038/ngeo2398>
- Brown, A. R. (1999). Large-eddy simulation and parametrization of the effects of shear on shallow cumulus convection. *Boundary-Layer Meteorology*, 91(1), 65–80. <https://doi.org/10.1023/a:1001836612775>
- Brucek, M., Nuijens, L., & Stevens, B. (2015). On the seasonal and synoptic time-scale variability of the north atlantic trade wind region and its low-level clouds. *Journal of the Atmospheric Sciences*, 72(4), 1428–1446. <https://doi.org/10.1175/jas-d-14-0054.1>
- Carr, M. T., & Bretherton, C. S. (2001). Convective momentum transport over the tropical pacific: Budget estimates. *Journal of the Atmospheric Sciences*, 58(13), 1673–1693. [https://doi.org/10.1175/1520-0469\(2001\)058<1673:cmott>2.0.co;2](https://doi.org/10.1175/1520-0469(2001)058<1673:cmott>2.0.co;2)
- Das, P. (1979). A non-archimedean approach to the equations of convection dynamics. *Journal of the Atmospheric Sciences*, 36(11), 2183–2190. [https://doi.org/10.1175/1520-0469\(1979\)036<2183:anaatt>2.0.co;2](https://doi.org/10.1175/1520-0469(1979)036<2183:anaatt>2.0.co;2)
- de Roode, S. R., Siebesma, A. P., Jonker, H. J. J., & de Voogd, Y. (2012). Parameterization of the vertical velocity equation for shallow cumulus clouds. *Monthly Weather Review*, 140(8), 2424–2436. <https://doi.org/10.1175/mwr-d-11-00277.1>
- Dee, D. P., Uppala, S. M., Simmons, A., Berrisford, P., Poli, P., Kobayashi, S., et al. (2011). The era-interim reanalysis: Configuration and performance of the data assimilation system. *Quarterly Journal of the Royal Meteorological Society*, 137(656), 553–597.
- Dipankar, A., Stevens, B., Heinze, R., Moseley, C., Zängl, G., Giorgetta, M., & Brdar, S. (2015). Large eddy simulation using the general circulation model icon. *Journal of Advances in Modeling Earth Systems*, 7(3), 963–986. <https://doi.org/10.1002/2015ms000431>
- Doswell, C. A., III, & Markowski, P. M. (2004). Is buoyancy a relative quantity? *Monthly Weather Review*, 132(4), 853–863. [https://doi.org/10.1175/1520-0493\(2004\)132<0853:ibarq>2.0.co;2](https://doi.org/10.1175/1520-0493(2004)132<0853:ibarq>2.0.co;2)

- Grant, L. D., Moncrieff, M. W., Lane, T. P., & van den Heever, S. C. (2020). Shear-parallel tropical convective systems: Importance of cold pools and wind shear. *Geophysical Research Letters*, 47(12), e2020GL087720. <https://doi.org/10.1029/2020gl087720>
- Gregory, D., Kershaw, R., & Inness, P. M. (1997). Parametrization of momentum transport by convection. II: Tests in single-column and general circulation models. *Quarterly Journal of the Royal Meteorological Society*, 123(541), 1153–1183. <https://doi.org/10.1002/qj.49712354103>
- Grubišić, V., & Moncrieff, M. W. (2000). Parameterization of convective momentum transport in highly baroclinic conditions. *Journal of the Atmospheric Sciences*, 57(18), 3035–3049.
- Helffer, K. C., Nuijens, L., de Roode, S. R., & Siebesma, A. (2020). How wind shear affects trade-wind cumulus convection. *Journal of Advances in Modeling Earth Systems*, 12(12). <https://doi.org/10.1029/2020ms002183>
- Helffer, K. C., Nuijens, L., & Dixit, V. (2021). The role of shallow convection in the momentum budget of the trades from large-eddy-simulation hindcasts. *Earth and Space Science Open Archive*, 19.
- Hernandez-Deckers, D., & Sherwood, S. C. (2016). A numerical investigation of cumulus thermals. *Journal of the Atmospheric Sciences*, 73(10), 4117–4136. <https://doi.org/10.1175/jas-d-15-0385.1>
- Heus, T., & Jonker, H. J. J. (2008). Subsiding shells around shallow cumulus clouds. *Journal of the Atmospheric Sciences*, 65(3), 1003–1018. <https://doi.org/10.1175/2007jas2322.1>
- Heus, T., van Heerwaarden, C. C., Jonker, H. J. J., Pier Siebesma, A., Axelsen, S., van den Dries, K., et al. (2010). Formulation of the Dutch Atmospheric Large-Eddy Simulation (DALES) and overview of its applications. *Geoscientific Model Development*, 3(2), 415–444. <https://doi.org/10.5194/gmd-3-415-2010>
- Houze, R. A., Jr (2014). *Cloud dynamics*. Academic Press.
- Kershaw, R., & Gregory, D. (1997). Parametrization of momentum transport by convection. I: Theory and cloud modeling results. *Quarterly Journal of the Royal Meteorological Society*, 123(541), 1133–1151. <https://doi.org/10.1002/qj.49712354102>
- Klocke, D., Brueck, M., Hohenegger, C., & Stevens, B. (2017). Rediscovery of the doldrums in storm-resolving simulations over the tropical atlantic. *Nature Geoscience*, 10(12), 891–896. <https://doi.org/10.1038/s41561-017-0005-4>
- Larson, V. E., Domke, S., & Griffin, B. M. (2019). Momentum transport in shallow cumulus clouds and its parameterization by higher-order closure. *Journal of Advances in Modeling Earth Systems*, 11(11), 3419–3442. <https://doi.org/10.1029/2019ms001743>
- LeMone, M. A. (1983). Momentum transport by a line of cumulonimbus. *Journal of the Atmospheric Sciences*, 40(7), 1815–1834. [https://doi.org/10.1175/1520-0469\(1983\)040<1815:mtbalo>2.0.co;2](https://doi.org/10.1175/1520-0469(1983)040<1815:mtbalo>2.0.co;2)
- LeMone, M. A., Barnes, G. M., & Zipser, E. J. (1984). Momentum flux by lines of cumulonimbus over the tropical oceans. *Journal of the Atmospheric Sciences*, 41(12), 1914–1932. [https://doi.org/10.1175/1520-0469\(1984\)041<1914:mfbloc>2.0.co;2](https://doi.org/10.1175/1520-0469(1984)041<1914:mfbloc>2.0.co;2)
- LeMone, M. A., & Moncrieff, M. W. (1994). Momentum and mass transport by convective bands: Comparisons of highly idealized dynamical models to observations. *Journal of the Atmospheric Sciences*, 51(2), 281–305. [https://doi.org/10.1175/1520-0469\(1994\)051<0281:mtb>2.0.co;2](https://doi.org/10.1175/1520-0469(1994)051<0281:mtb>2.0.co;2)
- List, R., & Lozowski, E. P. (1970). Pressure perturbations and buoyancy in convective clouds. *Journal of the Atmospheric Sciences*, 27(1), 168–170. [https://doi.org/10.1175/1520-0469\(1970\)027<0168:ppabic>2.0.co;2](https://doi.org/10.1175/1520-0469(1970)027<0168:ppabic>2.0.co;2)
- Moncrieff, M. W. (1978). The dynamical structure of two-dimensional steady convection in constant vertical shear. *Quarterly Journal of the Royal Meteorological Society*, 104(441), 543–567. <https://doi.org/10.1002/qj.49710444102>
- Moncrieff, M. W. (1981). A theory of organized steady convection and its transport properties. *Quarterly Journal of the Royal Meteorological Society*, 107(451), 29–50.
- Moncrieff, M. W. (1992). Organized convective systems: Archetypal dynamical models, mass and momentum flux theory, and parameterization. *Quarterly Journal of the Royal Meteorological Society*, 118(507), 819–850. <https://doi.org/10.1002/qj.49711850703>
- Moncrieff, M. W. (2010). The multiscale organization of moist convection and the intersection of weather and climate. *Climate Dynamics: Why Does Climate Vary?*, 189, 3–26. <https://doi.org/10.1029/2008gm000838>
- Moncrieff, M. W. (2019). Toward a dynamical foundation for organized convection parameterization in GCMS. *Geophysical Research Letters*, 46(23), 14103–14108. <https://doi.org/10.1029/2019gl085316>
- Moncrieff, M. W., & Liu, C. (2006). Representing convective organization in prediction models by a hybrid strategy. *Journal of the Atmospheric Sciences*, 63(12), 3404–3420. <https://doi.org/10.1175/jas3812.1>
- Moncrieff, M. W., Liu, C., & Bogenschutz, P. (2017). Simulation, modeling, and dynamically based parameterization of organized tropical convection for global climate models. *Journal of the Atmospheric Sciences*, 74(5), 1363–1380. <https://doi.org/10.1175/jas-d-16-0166.1>
- Morrison, H. (2016). Impacts of updraft size and dimensionality on the perturbation pressure and vertical velocity in cumulus convection. Part i: Simple, generalized analytic solutions. *Journal of the Atmospheric Sciences*, 73(4), 1441–1454. <https://doi.org/10.1175/jas-d-15-0040.1>
- Peters, J. M. (2016). The impact of effective buoyancy and dynamic pressure forcing on vertical velocities within two-dimensional updrafts. *Journal of the Atmospheric Sciences*, 73(11), 4531–4551. <https://doi.org/10.1175/jas-d-16-0016.1>
- Prill, F., Reinert, D., Rieger, D., Zaengl, G., Schroeter, J., Foerstner, J., et al. (2019). *Working with the icon model practical exercises for NWP mode and ICON-ART. ICON Model Tutorial*. Deutscher Wetterdienst.
- Rasp, S., Schulz, H., Bony, S., & Stevens, B. (2020). Combining crowdsourcing and deep learning to explore the mesoscale organization of shallow convection. *Bulletin of the American Meteorological Society*, 101(11), E1980–E1995. <https://doi.org/10.1175/bams-d-19-0324.1>
- Riehl, H. (1958). On the heat balance of the equatorial trough zone. *Geophysica*, 6, 503–538.
- Romps, D. M. (2012). On the equivalence of two schemes for convective momentum transport. *Journal of the Atmospheric Sciences*, 69(12), 3491–3500. <https://doi.org/10.1175/jas-d-12-068.1>
- Romps, D. M., & Charn, A. B. (2015). Sticky thermals: Evidence for a dominant balance between buoyancy and drag in cloud updrafts. *Journal of the Atmospheric Sciences*, 72(8), 2890–2901. <https://doi.org/10.1175/jas-d-15-0042.1>
- Rotunno, R., & Klemp, J. B. (1982). The influence of the shear-induced pressure gradient on thunderstorm motion. *Monthly Weather Review*, 110(2), 136–151. [https://doi.org/10.1175/1520-0493\(1982\)110<0136:tiotsi>2.0.co;2](https://doi.org/10.1175/1520-0493(1982)110<0136:tiotsi>2.0.co;2)
- Schlemmer, L., Bechtold, P., Sandu, I., & Ahlgrimm, M. (2017). Uncertainties related to the representation of momentum transport in shallow convection. *Journal of Advances in Modeling Earth Systems*, 9(2), 1269–1291. <https://doi.org/10.1002/2017ms000915>
- Schneider, E. K., & Lindzen, R. S. (1976). A discussion of the parameterization of momentum exchange by cumulus convection. *Journal of Geophysical Research*, 81(18), 3158–3160. <https://doi.org/10.1029/jc081i018p03158>
- Sherwood, S. C., Hernández-Deckers, D., Colin, M., & Robinson, F. (2013). Slippery thermals and the cumulus entrainment paradox. *Journal of the Atmospheric Sciences*, 70(8), 2426–2442. <https://doi.org/10.1175/jas-d-12-0220.1>

- Siebesma, A. P., Bretherton, C. S., Brown, A., Chlond, A., Cuxart, J., Duynkerke, P. G., et al. (2003). A large eddy simulation intercomparison study of shallow cumulus convection. *Journal of the Atmospheric Sciences*, *60*(10), 1201–1219. [https://doi.org/10.1175/1520-0469\(2003\)60<1201:alesis>2.0.co;2](https://doi.org/10.1175/1520-0469(2003)60<1201:alesis>2.0.co;2)
- Siebesma, A. P., & Cuijpers, J. W. M. (1995). Evaluation of parametric assumptions for shallow cumulus convection. *Journal of the Atmospheric Sciences*, *52*(6), 650–666. [https://doi.org/10.1175/1520-0469\(1995\)052<0650:eopafs>2.0.co;2](https://doi.org/10.1175/1520-0469(1995)052<0650:eopafs>2.0.co;2)
- Stevens, B., Ament, F., Bony, S., Crewell, S., Ewald, F., Gross, S., et al. (2019). A high-altitude long-range aircraft configured as a cloud observatory: The narval expeditions. *Bulletin of the American Meteorological Society*, *100*(6), 1061–1077. <https://doi.org/10.1175/bams-d-18-0198.1>
- Stevens, B., Bony, S., Brogniez, H., Hentgen, L., Hohenegger, C., Kiemle, C., et al. (2020). Sugar, gravel, fish and flowers: Mesoscale cloud patterns in the trade winds. *Quarterly Journal of the Royal Meteorological Society*, *146*(726), 141–152. <https://doi.org/10.1002/qj.3662>
- VanZanten, M. C., Stevens, B., Nuijens, L., Siebesma, A. P., Ackerman, A., Burnet, F., et al. (2011). Controls on precipitation and cloudiness in simulations of trade-wind cumulus as observed during rico. *Journal of Advances in Modeling Earth Systems*, *3*(2). <https://doi.org/10.1029/2011ms000056>
- Wu, X., & Yanai, M. (1994). Effects of vertical wind shear on the cumulus transport of momentum: Observations and parameterization. *Journal of the Atmospheric Sciences*, *51*(12), 1640–1660. [https://doi.org/10.1175/1520-0469\(1994\)051<1640:eovwso>2.0.co;2](https://doi.org/10.1175/1520-0469(1994)051<1640:eovwso>2.0.co;2)
- Zängl, G., Reinert, D., Ripodas, P., & Baldauf, M. (2015). The ICON (ICOsahedral Non-hydrostatic) modelling framework of DWD and MPI-M: Description of the non-hydrostatic dynamical core. *Quarterly Journal of the Royal Meteorological Society*, *141*(687), 563–579. <https://doi.org/10.1002/qj.2378>
- Zhang, G. J., & Cho, H.-R. (1991). Parameterization of the vertical transport of momentum by cumulus clouds. Part i: Theory. *Journal of the Atmospheric Sciences*, *48*(12), 1483–1492. [https://doi.org/10.1175/1520-0469\(1991\)048<1483:potvto>2.0.co;2](https://doi.org/10.1175/1520-0469(1991)048<1483:potvto>2.0.co;2)
- Zhu, P. (2015). On the mass-flux representation of vertical transport in moist convection. *Journal of the Atmospheric Sciences*, *72*(12), 4445–4468. <https://doi.org/10.1175/jas-d-14-0332.1>